

Effect of Multiple Through-Holes on the Turbine Blade Trailing Edge

[Mohd Hafiz Mohd Noh, Koichi Mori]

Abstract—The vortex shedding of a turbine blade is suppressed by making hole, connecting between the pressure side and suction side in the area of the trailing edge. Computational work is carried out using the numerical code developed in house. A Spalart–Allmaras turbulence model with Delayed Detached Eddy Simulation is used. The exit Reynolds number is 2.8×10^6 and the exit isentropic Mach number is 0.79. Three hole diameters are being investigated: $0.054D$, $0.065D$ and $0.094D$. Hole diameter of $0.094D$ is the best configuration, where the result shows that the wake loss reduces by a maximum of 10%, the pressure distribution along trailing edge has increased by 14% and the wake profile thickness reduces at maximum of 24% as compared with no hole blade. The wake loss is sensitive to the size and location of the hole.

Keywords—Turbine Blade, Pressure Distribution, Numerical Investigation, Vortex Shedding, Wake Loss

I. Introduction

A number of studies have been devoted to improve the performance of a gas turbine by minimizing component losses such as wake loss, profile loss, secondary loss, tip clearance loss and annulus loss [1,2]. Losses can be reduced via the optimum design of the blade geometry (shape) and by employing additional flow control techniques [3]. The turbine blade wakes have an unsteady characteristic that is originated from the large-scale organized structures in vortex streets, in the form of vortex shedding. The vortex shedding contributes different loss mechanisms. The total loss from the vortex shedding is generally important under high-speed conditions [4].

One of the active flow control technique used to suppress vortex shedding involves jets, such as plasma actuators and synthetic jets [5,6]. Optimization of the blade geometry is another way of suppressing vortex shedding. Zhou et al., investigated the effect of the trailing edge thickness on vortex shedding [7].

Dwayne et al., found that a thicker trailing edge tended to increase the vortex shedding strength [8]. Bearmen et al., tested a so-called ‘splitter plate’ at the trailing edge [9].

In this paper, we propose a method of suppressing vortex shedding by connecting the pressure side and suction side via micro holes. In previous studies, the pressure loss of the blade was suppressed by making holes on the blade. Yangwei et al., found that the total pressure loss and the passage blockage were reduced by making a suction slot on the blade [10]. The pressure distribution on the blade has been increased by injecting cold air through holes to cool the film [11]. The pressure along trailing edge has been increased by making a 0.1-mm hole, connecting the suction side and pressure side of the blade [12]. In these foregoing studies, the simulation only considered that the hole being a single point on the blade-spanwise, and the location and size of the hole were not optimized. Thus, this paper focuses on the effect of the size and location of the multiple micro holes at trailing edge region on the wake vortex shedding.

II. Computational Method

The three-dimensional, Reynolds-averaged, unsteady Navier–Stokes equation is solved. The numerical model consists of the continuity equation, three dimensional Navier–Stokes equations for compressible flow. The inviscid fluxes are discretized using the total variation diminishing scheme and viscous fluxes are discretized using standard central differences. The configuration of the cascade is presented in Fig. 1, where the chord length, C is 140 mm, axial chord length, C_{ax} is 91.84 mm and pitch, s is 97.44 mm. The span-wise size of the blade is 10% of the blade chord length and trailing edge diameter, $D = 7.48$ mm. S is the length measured along the trailing edge surface line.

Mohd Hafiz Mohd Noh
Nagoya University
Japan
hafiz@fluid.nuae.nagoya-u.ac.jp, mhafiz_noh@yahoo.com

Koichi Mori
Nagoya University
Japan
mori@fluid.nuae.nagoya-u.ac.jp

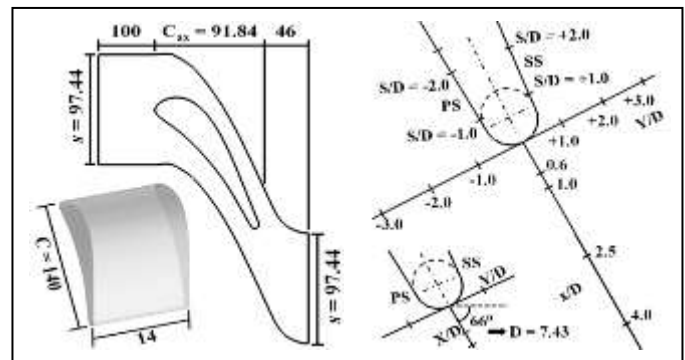


Figure 1. Blade configuration and dimensions (in mm)

Figure 2. Trailing-edge S/D , x/D and Y/D reference system

The in-house code that used in this calculation is structured, single block and second-order accurate in time. Roe's flux-difference splitting scheme is used for a numerical inviscid flux calculation, where second-order accuracy is achieved employing the MUSCL scheme with the van Albada flux limiter and the lower upper symmetric Gauss Seidel together with a second-order dual time stepping method is employed to calculate the unsteady flow.

Fig. 2 shows a close-up view of the region around the trailing edge and the definitions of x/D and Y/D . The maximum number of iterations is 2×10^6 , and there are five inner iterations for the implicit scheme (time marching). Dimensionless Δt^* is equal to 105.42×10^{-6} and the physical time step $\Delta t = 3.33 \times 10^{-7}$ s. The numerical method is validated by comparing the numerical results with experimental data obtained by Sieverding et al., for the configuration without a hole [13,14]. The Courant–Friedrichs–Lewy number is around 10.

A. Boundary Conditions

Fig. 3 shows an O-type structured grid that has $413 \times 194 \times 50 (= 4.0 \times 10^6)$ grid points. For pre-processing, the grid has been developed via Gridgen Version 15 software. The minimum grid size is 0.002mm which is equivalent to $y^+ \approx 1$. On the blade surface, a non-slip adiabatic wall boundary condition is applied. Subscripts "01" and "02" are refers to the inlet and outlet condition, while subscripts "in" and "out" are represented inside and outside the calculation domain. Imposed boundary conditions at the turbine inlet are total pressure, $P_{01} = 140,000\text{Pa}$ and total temperature, $T_{01} = 280\text{K}$, respectively. For inlet boundary condition, subsonic Riemann Invariant condition, R_{01} has been imposed, where [15];

$$R_{01} = \overline{V_{in}} \cdot \vec{n} - 2 \left[\frac{c_{in}}{\gamma - 1} \right] \quad (1)$$

V_{in} is velocity vector, c is speed of sound, γ is specific heat ratio (1.4) and n is normal vector on inlet plane. With this, we can calculate the velocity V_{01}

$$V_{01} = \frac{-R_{01} - (\gamma - 1)}{(\gamma - 1) \cos^2 \theta + 2} \left\{ 1 + \cos \theta \sqrt{A_1 - A_2} \right\} \quad (2)$$

where;

$$A_1 = \frac{[(\gamma - 1) \cos^2 \theta + 2] c_0^2}{(\gamma - 1) R_{01}^2} \quad \text{and} \quad A_2 = \left[\frac{\gamma - 1}{2} \right] \quad (3)$$

where θ is the flow angle relative to the inlet boundary [15]. The speed of sound at stagnation condition, c_0 can be obtained by

$$c_0 = c_{in}^2 + \frac{\gamma - 1}{2} (\overline{V_{in}})^2 \quad (4)$$

Translational periodical boundary condition is applied for this calculation as illustrated in Fig. 3 as in previous studies [16,17,18]. At the outlet, isentropic Mach number $M_{is,02} = 0.79$ and the Reynolds number is 2.8×10^6 , which is same as reference [13,14]. To achieve this conditions, the outlet total

pressure is specified as $P_{02} = 92,755 \text{ Pa}$ (5). Based on this condition, outlet static pressure $P_{s,02}$ and outlet static temperature $T_{s,02}$ have been calculated via;

$$P_{s,02} = P_{01} \left(1 + \frac{\gamma - 1}{2} M_{is,02}^2 \right)^{-\left(\frac{\gamma}{\gamma - 1} \right)} \quad (5)$$

$$T_{s,02} = T_{01} \left(1 + \frac{\gamma - 1}{2} M_{is,02}^2 \right)^{-1} \quad (6)$$

subscript "is" is refer to isentropic. At the outlet, the static pressure P_{02} has been prescribed. Subsonic outlet boundary condition and entropy relation has been imposed, which has been calculated by (7), so subsonic Riemann Invariant condition at outlet, R_{02}

$$R_{02} = \overline{V_{out}} \cdot \vec{n} + 2 \left[\frac{c_{out}}{\gamma - 1} \right] \quad (7)$$

with outlet pressure has been specified (in dimensionless form), so the density, ρ_{02} and velocity V_{02} can be obtained by;

$$\rho_{02} = \left[\frac{P_{02}}{P_{in}} \right]^{\left(\frac{1}{\gamma} \right)} \quad (8)$$

$$V_{02} = R_{02} - 2 \left[\frac{c_{02}}{\gamma - 1} \right] \quad (9)$$

The flow through each micro-hole is modeled using the Hagen–Poiseuille equation [12];

$$U = \frac{R^2}{4\mu} \left[- \frac{\Delta P}{\Delta L} \right] \quad (10)$$

where U is the velocity through the hole, R is the radius of the hole, μ is the viscosity, ΔP is the pressure difference across the micro-hole and ΔL is the tube length. Even this equation was not explicitly being checked since not much research has been conducted by using (10) in turbomachinery fluid dynamics research, but it being widely used in other research field i.e morphology and biology for calculating blood flow and capillary flow [19,20,21]. In turbine calculation, up to date, this relation first has been introduced by El. Gendi et. al., [12]. There are several assumptions have been made in respect to the (10).

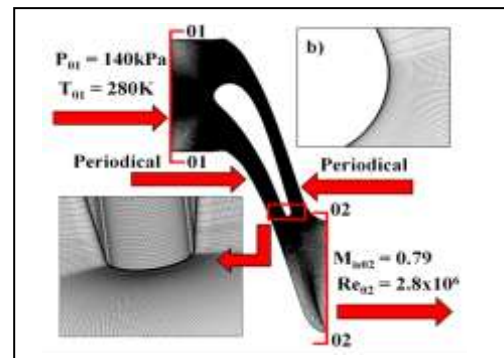


Figure 3. Boundary conditions and simulation grid b) Close view of grid at micro-holes area

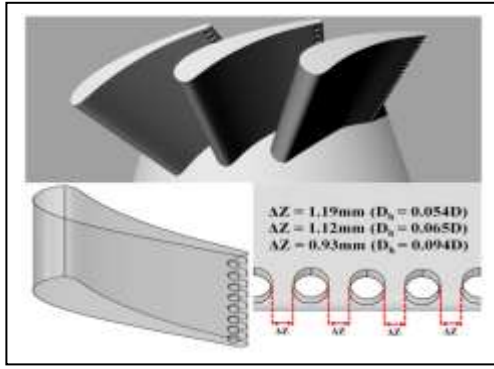


Figure 4. Connecting holes at the trailing edge of the blade

First, since the hole size in this study is in micrometer size, so the effect inside the hole is assumed to be laminar, incompressible, fully developed and steady [12]. This U affected mass, momentum and energy conservation. After validation, the micro-hole is applied in the area of the trailing edge of the studied blade as illustrated in Fig. 4. The number of holes has been fixed to be eight (8) for all the cases.

B. Turbulence Models

Four turbulence models have been tested, which are Spalart Allmaras (SA), Detached Eddy Simulation (DES), Delay Detached Eddy Simulation ($DDES$) and Improved Delay Detached Eddy Simulation ($IDDES$) turbulence models [22,23,24,25]. The Spalart Allmaras model is a transport equation model for the eddy viscosity. The equation for viscosity $\tilde{\nu}$ can be defined by this followings expression;

$$\frac{D\tilde{\nu}}{Dt} = \underbrace{c_{b1}\tilde{S}\tilde{\nu}}_{Production} + \underbrace{\frac{1}{\sigma}[\nabla \cdot ((\nu + \tilde{\nu})\nabla\tilde{\nu}) + c_{b2}(\nabla\tilde{\nu})^2]}_{Diffusions} - \underbrace{c_{w1}f_w\left(\frac{\tilde{\nu}}{d}\right)^2}_{Destruction} \quad (11)$$

subscript b here stands for basic, d is the distance to the closest wall, \tilde{S} is local deformation rate, ν is molecular viscosity, $\tilde{\nu}$ is the working variable that satisfied the above equation [22]. All the remaining parameters has been described in detail in the references [22,23].

DES has been developed in order to deal with higher Reynold number, was originally formulated by [24]. DES turbulence model is a hybrid scheme, where it works as $RANS$ near the wall and works as LES away from wall including separated boundary layer and wake. For $RANS$, the spatial Favre filtered compressible Navier-Stokes equations are used. In LES , the original Smagorinsky model is used for sub-grid-scale (SGS) modeling for small eddy [26,27]. As described before, the destruction part of SA turbulence model contains $\tilde{\nu}/d^2$. As this term balance with the production term, so $\tilde{\nu}$ become proportional to S and d^2 . The SGS scale $\tilde{\nu}$ together with S and grid spacing Δ , become $\nu_{SGS} \propto [S\Delta^2]$ [24]. So here the initial idea of DES has been discovered with C_{DES} is adjustable parameter of 0.65. DES works by replacing the length scale in the SA turbulence model d by a new length scale \tilde{d}

$$\tilde{d} = \min(d, \Delta C_{DES}) \quad (12)$$

where $\Delta = \max(\Delta_x, \Delta_y, \Delta_z)$ are local maximum grid spacing. So with this new \tilde{d} , DES is able to control the eddy viscosity. Near the blade surface, $\tilde{d} = d$ and otherwise $\tilde{d} = \Delta C_{DES}$. Due to the fact that the length scale only depends on the grid spacing, problems can arise if the grid spacing (in wall-normal) is finer than boundary layer thickness [25]. In this case, the local maximum grid spacing Δ becomes smaller than the wall distance d in the boundary layer. In order to solve this problem, $DDES$ has been introduced. Since in the Spalart-Allmaras model, it does not have an internal length scale, so the parameter r_d is introduced. The SA model with $DDES$ is defined as [25]

$$f_d = 1 - \tanh(\beta r_d)^3 \quad \text{where } r_d = \frac{\nu_T + \nu}{\sqrt{u_{ijk}u_{ijk}}\kappa^2 d^2} \quad (13)$$

where u_{ijk} is velocity profile and f_d is 1 in the LES region where $r_d \ll 1$ and zero in the $RANS$ region [25]. κ is von karman constant (0.41) and ν_T is kinematic eddy viscosity. Eventually, new length scale, d_{DES} can be redefined as;

$$d_{DES} = d - f_d \max(0, d - C_{DES}\Delta) \quad (14)$$

Therefore, at the boundary layer ($f_d = 0$), d_{DES} is equal to d . For $RANS$ simulation, outside of the boundary layer and separated flow region, d_{DES} behaves like classical DES . $IDDES$ is further improvement of $DDES$, where parameter r_d is defined as

$$r_{d,iddes} = \frac{\nu_T + \nu}{\kappa^2 d^2 \max\left\{ \left[\sum_{ijk} u_{ijk}u_{ijk} \right] \right\}^{1/2}, 10^{10}} \quad (15)$$

The major differences of $DDES$ and $IDDES$ from others that it requires more computational cost, at the same time, beneficial in term of less requirement of fine grid near the wall. As compared with DES , $DDES$ estimate $RANS$ by flow and grid size, which DES depend on grid size only. All the calculation results are compared with the experimental value and have been presented in the result and discussion section on this paper.

III. Result and Discussion

A. CFD Code Validation

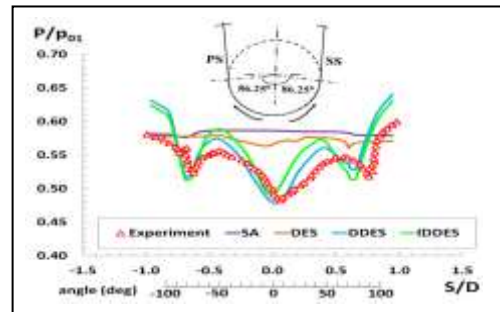


Figure 5. Trailing edge pressure distribution comparison between four difference turbulence models and experiment data

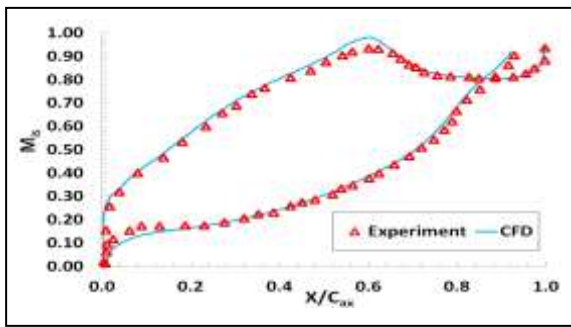


Figure 6. Comparison of the isentropic Mach the blade

Each turbulence model has been compared in term of trailing edge pressure distribution respect to the experimental result [13,14]. Fig. 5 shows the comparison result of each turbulence model. As we can see, *SA* model cannot capture the minimal pressure as compared with others. This can be explained as in the *SA* model destruction part, the d is solely depend on grid size so if any viscous appeared lower than Δ , so the modification of length scale need to be done. Potsdam et. al has confirmed that non modified *SA* model has problem when dealing with highly vertical flow [28]. So it can be said that, d cannot be calculated as conventional way.

As *DES* being implemented, we can see little improvement in capturing the pressure drop on the surface, but still insufficient to give close result to the experiment. Apparently, *DDES* and *IDDES* turbulence model give good closes result to the experiment. So based on this finding, *DDES* turbulence has been selected to use in this calculation, which was also being suggested by previous research [12,25,29]. Magagnato et. al., has found that *DDES* (together with Abu Ghananam and Shaw correlation) was capable to capture the insipient separation in transitional flow prediction on turbine blade as compared with *LES* [30]. So, it proven that *DDES* turbulence model has good choice to apply in turbine blade study.

The present computation produced three local minimum values of dimensionless pressure, which also appeared in the experimental results (at $S/D \approx -0.7, 0.0$ and 0.75). The locations of these minimal points and the minimum values of the computed results agree well with the experimental results. Sieverding et al., claimed that, at this pressure plateau (after the pressure minima values), there are separations due to overexpansion of the suction and pressure sides [13]. This is one of the reasons for the discrepancy between the present results and the experimental results at $|S/D| > 0.8$.

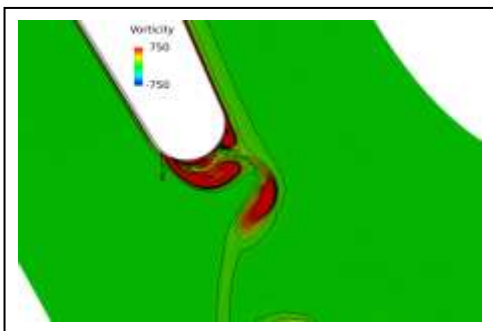


Figure 7. Instantaneous vorticity contour in the wake of the blade

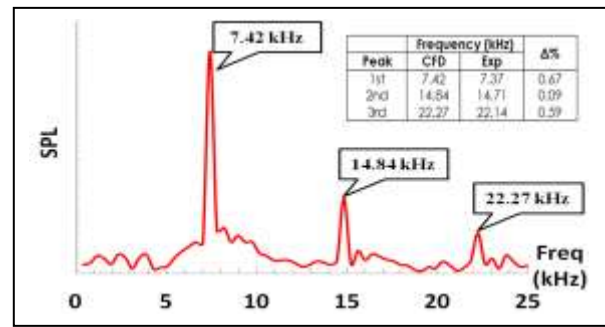


Figure 8. Pressure Spectra at $S/D = -0.62$

Fig. 6 shows the isentropic Mach number. The numerical results agree well with experimental results. In order to decide the location of the hole, we observe the flow field near the trailing edge of the blade (no hole) and also the Fast Furious Transformation (FFT) calculation has been tabulated at the respective location. FFT shall give the information about the dominant frequency at the chosen hole's location and also give an indication whether our flow calculation captured the flow field in a timely accurate manner.

Friedrichs et al., (1999) has made holes in regions of high static pressure to reduce aerodynamic penalties. The vortices should be suppressed by making holes near the location of vortex shedding [31]. Fig. 7 shows the instantaneous vorticity contour in the wake of the blade. The initial vortex shedding begins at $S/D = -0.62$. This result is consistent with Lake's results that the vortex shedding of the Pak-B blade starts at about 70% of the normalized axial [1]. FFT also shows that predominance frequency occurred at $S/D = -0.62$, as shown if Fig. 8. Spectral Pressure Level (SPL) of the graph shows a peak at 7.42kHz, which is consistent with the reference [13,14]. The comparison between computational and experiment of the initial of three frequency peak also agree well for each other.

Validation also been done for boundary layer characteristics. Boundary layer profiles were measured at distance equal to one trailing edge diameter for both suction side and pressure side. Fig. 9 shows the result of this comparison, where a good agreement has been achieved between experiment and computational results.

B. Velocity Profile Thickness

Table I summarizes the three sizes of hole used for investigation at constant $S/D = \pm 0.62$. "Base" represents the basic blade without any hole.

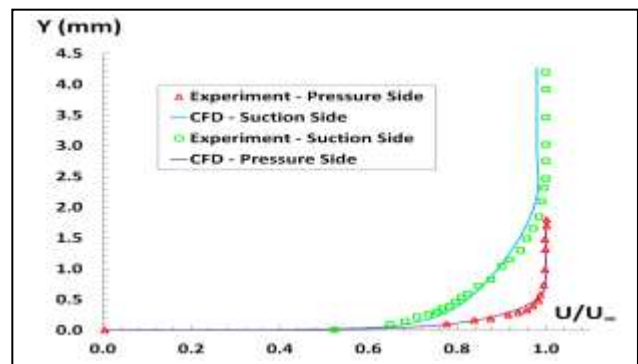


Figure 9. Boundary layer profile at trailing edge

TABLE I. HOLE DIAMETERS AT CONSTANT $S/D = \pm 0.62$

D_h/D	L/D_h
Base	-
0.054	18.12
0.065	15.23
0.094	10.32

L is length of the hole and D_h is hole diameter. The velocity profile is plotted in Fig. 10. The unity velocity is defined at the point where the profile velocity (u/u_{max}) remains unchanged with a further increase in y/D . The profile thickness is measured according to the distance between the point where the velocity become unity and the point of maximum velocity (for both suction and pressure sides). The velocity profile thickness is less in all cases with holes than in the base case. The results are summarized in Table II.

Table II compares the thickness of the velocity profile in each case. The base cascade (no hole) shows growth in the profile thickness downstream from $x/D = 2$ to $x/D = 4$. This wake growth is due to turbulence mixing. When the hole is added at $S/D = \pm 0.62$ on the blade, the velocity profile thickness reduces dramatically. For the smallest D_h ($0.054D$), the profile thickness reduces by 14%.

As D_h increases from $0.054D$ to $0.065D$, the profile thickness further decreases by nearly 20%. For $D_h = 0.094D$, the profile thickness further decreases by 24%. According to (10), an increase in D_h may lead to an increase in U . As U increased, the mixing and momentum increase [32]. The increase in momentum affects the overall velocity. This explains why $D_h = 0.094D$ gives the smallest thickness of the velocity profile. This result is supported by previous results [33]. The average velocity in the wake region is lower in the hole cases, which demonstrates good flow control. Furthermore, creating a hole does not affect the velocity component u at the center of the wake region ($-0.4 < Y/D < +0.4$); this finding is in line with previous results [34].

C. Total Pressure

Fig. 11 shows the time-averaged total pressure contour in the wake for different values of D_h . Obviously, the pressure drop is reduced and the vortex suppressed by adding the hole. Initially, the pressure drop for the base case has dominance in the center region of the wake ($-1 < y/D < +1$), until $x/D = 10$ as shown in Fig. 11(a). For $D_h = 0.054D$, the pressure drop is minimized to $x/D = 8$, approximately. As D_h increases from $0.054D$ to $0.065D$, the pressure drop in the wake decreases as the length of x/D decreases - Fig. 11(c). For $D_h = 0.094D$, this pressure drop further reduces.

TABLE II. VELOCITY PROFILE THICKNESS FOR DIFFERENT HOLE DIAMETERS AT (A), (B) AND (C)

D_h/D	(a) $x/D = 2$	(b) $x/D = 3$	(c) $x/D = 4$
Base	3.60	3.76	3.92
0.054	3.60	3.50	3.10
0.065	3.60	3.30	2.90
0.094	3.30	3.20	2.50

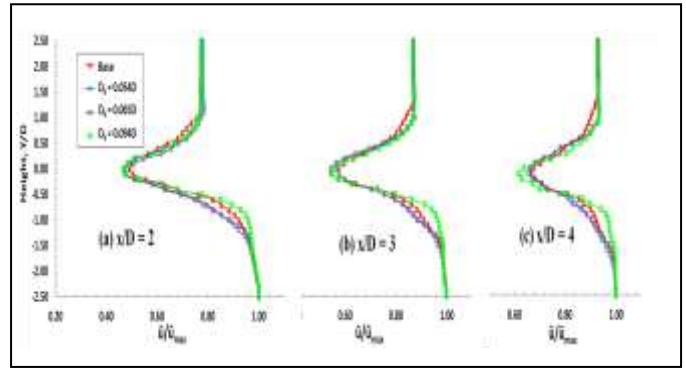


Figure 10. Velocity profile at the blade wake for different hole diameters at (a), (b) and (c)

The pressure relaxation is achieved more rapidly for larger D_h . This can be explained as follows. In this study, the hole is represented in terms of the dimensionless velocity (10). A change in D_h affects U and pressure, as confirmed by previous results [18]. The hole changes the flow stream, resulting in propagation of the local vortex and a decrease in pressure in the wake. This is why total pressure drop at $D_h = 0.094D$ been suppressed at shorten x/D .

Further downstream in the wake (from $x/D = 0$ to $x/D = 10$), the interaction between flows from the suction and pressure sides continues, reducing the pressure. Fig. 12 shows the distribution of the trailing edge pressure at different values of D_h . An increment in pressure will reduce the wake loss and enhances the overall performance [35,36,37]. Obviously, the trailing edge pressure increases in all cases that there is holes in blade, which is confirmed by previous results [12]. The trends for $D_h = 0.054D$ and $D_h = 0.065D$ are similar. For $D_h = 0.094D$, the pressure is a maximum of 14% greater than that in the base case.

As explained earlier, U increases as D_h increases. Because the pressure in this study is slightly higher than ambient pressure, the changes in cross flow velocity are related to the mean free path. The mean free path is the average distance of motion of a moving particle and is related to the diameter of the molecule, relative velocity and pressure.

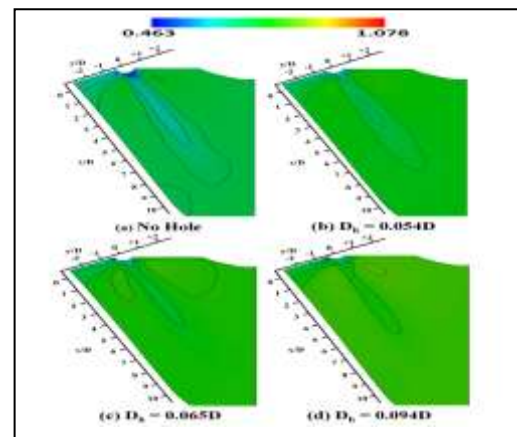


Figure 11. Time-averaged total pressure contour at the blade wake for different hole diameters

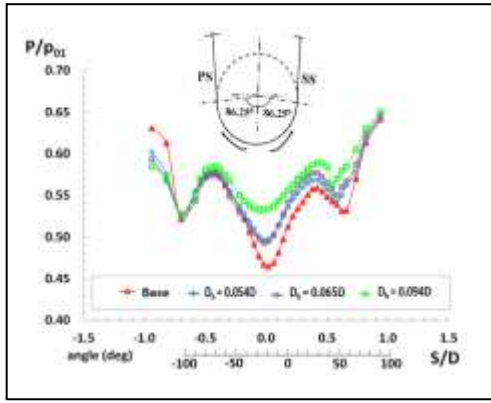


Figure 12. Distribution of trailing edge pressure along the trailing edge

As the velocity increase, the mean free path reduces in length. Since the number of molecules per unit volume can be determine from the ideal gas law, the shorter mean free path means higher pressure. This is why a larger D_h results in higher pressure. Connecting the pressure and suction sides of the blade shifts the pressure from the high-pressure region to the low-pressure region. As a result, the pressure increases in the low-pressure region, which offsets the shear layer in this area. This weakens the vortex on the blade surface and reduces the pressure drop in the wake. According to (10), if density, μ and L are assumed constant, then U is only a function of the pressure difference, ΔP and hole size, R . As D_h increases, the velocity also increases. An increment of U should increase the pressure for a certain D_h , which could explain the increase in pressure with increasing hole size.

D. Wake Loss

The wake loss, ζ is defined as

$$\zeta = \frac{P_{01} - P_{02}}{P_{01} - P_{s,02}} \quad (14)$$

where P_s is the static pressure. All pressure values are time averaged. Fig. 13 shows the wake loss coefficients for different values of D_h . By plotting the wake loss, the reduction of the pressure loss can be viewed. Overall, it is clear that ζ is lower in the case of a hole than for the base blade. All graphs have a peak at $Y/D = 0$.

The case of $D_h = 0.054D$ has a trend similar to that of the base case. An increase in D_h from $0.054D$ to $0.065D$ has decreases ζ by approximately 2% at the center of the wake region. At the same time, ζ increases in the $Y/D > 0.4$ region and $-0.8 < Y/D < -0.4$ region. The reduction of ζ is greater when $D_h = 0.094D$. In the center region of the wake ($-1 < Y/D < 1$), wake loss is minimized by a maximum of 10% relative to the base case. The reduction of ζ is related to the increase in pressure produced at the exit of the blade, which was explained previously. As we integrate each curve respect to the minimum and maximum of Y/D value, it obvious to see that $D_h = 0.094D$ give the lowest percentage of ζ .

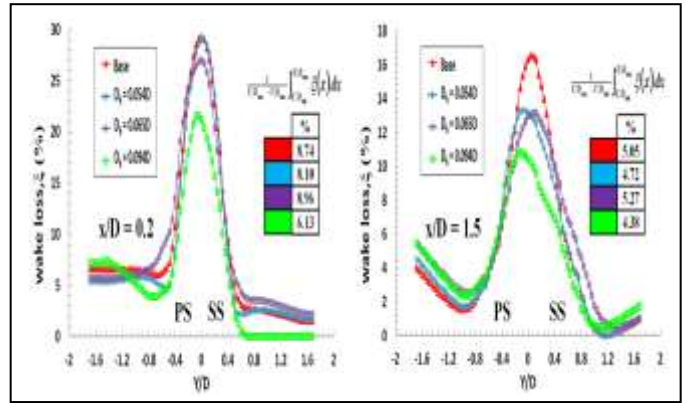


Figure 13. Wake loss coefficients at $x/D = 0.2$

Figure 14. Wake loss coefficients at $x/D = 1.5$

In a physical sense, the presence of the hole increases the surface area. The fluid thus experiences more friction, which may contribute to large loss. As a result, the pressure drop at the hole surface is reduced. The surface pressure is thus higher for a blade with a hole than for the blade with no hole. In contrast, there is a small increase in ζ at $Y/D < -1.2$ for $D_h = 0.094D$. This increase is related to the shifted shear boundary layer in a low-pressure region on the surface, and may result in a pressure drop in the field far from the blade's wall and not full suppressed at a short distance of x/D .

As mentioned before, the vortex of a blade with hole is suppressed more rapidly than the base blade. Fig. 14 shows ζ at $x/D = 1.5$. The lowest ζ is observed for $D_h = 0.094D$, which suggests that there is high pressure in this plane ($x/D = 1.5$). All cases of a blade with hole have low ζ at a short x/D distance, indicating that a hole directly affects the total pressure produced in the wake. It can be said that D_h affects the trailing edge pressure and wake loss.

Eventually, $D_h = 0.094D$ was chosen for the optimum value for further investigation. While maintaining $D_h = 0.094D$, the location of the hole is changed and the effect of ζ investigated. Table III summarizes the variation of S/D at constant D_h . The relationship between the hole location and ζ is presented in Fig. 15 and Fig. 16. For $S/D = \pm 0.73$, ζ is similar to that in the base case (in the center region of the wake). This can be explained by the fact that there is no initial vortex formation at this location ($S/D = \pm 0.73$). Creating hole at this location may have a small effect on the closes flow stream (near the blade surface) and pressure drop.

As the hole location shifts to $S/D = \pm 0.58$, ζ decreases. At $S/D = \pm 0.58$, the trend of ζ is similar to that for $S/D = \pm 0.62$. This is because there is an initial vortex in this area, and the addition of the hole thus delays the vortex formation and reduces ζ .

TABLE III. VARIATION OF S/D AT A CONSTANT HOLE DIAMETER ($D_h = 0.094D$)

S/D	L/D _h
Base	-
± 0.58	11.02
± 0.62	10.32
± 0.73	9.69

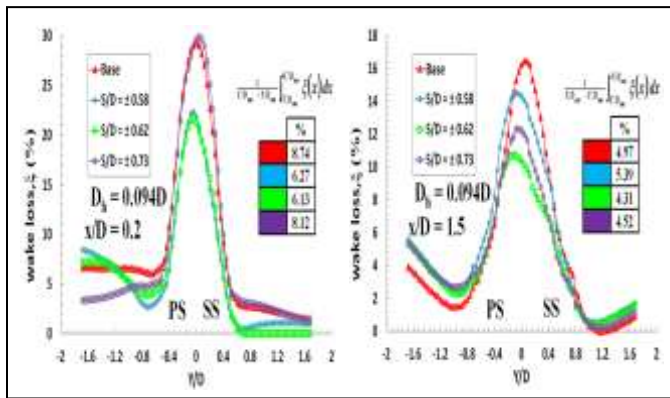


Figure 15. Wake loss coefficients at $x/D = 0.2$

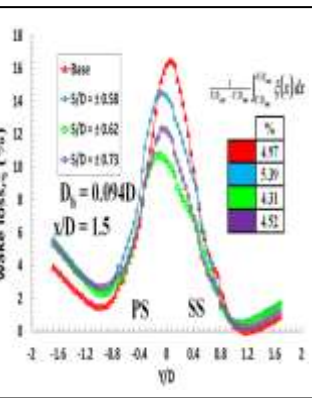


Figure 16. Wake loss coefficients at $x/D = 1.5$

A maximum of 2.61% of reduction in ζ has been achieved in this calculation (average). There are discrepancies in the $Y/D < 0$ region between each case. This is because the hole is added near the initial vortex. The effect of the pressure increment on the low-pressure side thus moves the boundary layer near the blade surface, pushes the nearest vortex downstream with minimum energy dissipation, and reduces the pressure in this area. The hole also delays the vortex formations, thus weakening the vortices. This results in the ideal pressure becoming dominant, thus reducing the pressure loss through the hole and reducing the pressure drop in the wake.

The vortex cannot be suppressed at a short distance x/D . An observation further downstream is thus needed. Fig. 16 presents ζ for different locations at $x/D = 1.5$. Further downstream, the discrepancies of ζ in the $Y/D < 0$ region are eliminated. The base case still produces the highest ζ . On this plane, the difference between $S/D = \pm 0.73$ and the base case is appreciable, in contrast with previous observations at $x/D = 0.2$.

The case of $S/D = \pm 0.62$ continues to produce the lowest ζ . At $S/D = \pm 0.62$, the vortex formation is delayed, which affects vortex formation downstream of the cascade. This shows that a series of micro-hole at the location of vortex formation not only increases the trailing edge pressure distribution but also reduces ζ . This effect may also be due to the lower L/D_h as reviewed by Bunker, who stated that lower L/D may improve the pressure distribution and reduce the overall energy loss [38]. Modification at the location of the dominant vortex affects the pressure and reduces the energy loss. It can be said that ζ is affected not only by the hole diameter but also the hole location.

E. Instantaneous flow field

The instantaneous iso-surface of the study case has been plotted in order to show better comparison (in term of flow field) between the base case and hole case. Fig. 17 shows iso-surfaces of vorticity magnitude colored with streamwise velocity. The isometric view has been oriented, which permits the observation of wake vorticity and shear layer, plus the effect of the hole mechanisms. Via this figure, we can also see the gradual shedding of the vortex. The comparison has been

made approximately at the same time phase. The $D_h = 0.094D$ at $S/D = \pm 0.62$ has been chosen for this configuration.

Fig. 17(i) correspond to the initial condition of wake vortex formation for base and hole case. The difference between both case are readily apparent even at early stage. There are vortices concentrations at the trailing edge surface area of the base case, which it doesn't significantly notify at the span-wise hole oriented case. Also at this stage, the starting of enrollment of vortex shedding from the pressure side of the blade still doesn't exist in both cases. As the holes added to the surface of the blade, the vortex has suppressed around trailing edge (at the region downstream of hole area) and reduced the vortex concentration (at hole area). In short, the addition of micro-hole has successfully suppressed the strong vortex at the surface of trailing edge surface.

For Fig. 17(ii), attention should be addressed at the trailing edge area of the blade. In the base case, there are strong vortex remained on the surface of the blade. While for hole case, at this phase, the vortex has been gradually reduced. Also, for hole case, at the region between the hole downstream area ($-0.62 < S/D < +0.62$), less strong vortex has been developed, which not appeared in the base case. This is believed due to the vortex from pressure side start to enroll and mixed with suction side vortex. At the same time, the vortex starts to grow and move away from trailing edge. The initial development of downstream vortex has started and both cases (base and hole) have approximate produce the same size of vortex.

The significant difference has been observed via Fig. 17(iii). While micro-hole series has continued induced strong vortex, make "second vortices" downstream at the wake has been separated from the initial vortex formation. While for the base case, "second vortices" is not fully separated with initial vortex. Further downstream of the wake, we can observe the growth of vortex shedding for both cases. For hole case, this growth has been significantly being reduced, which has been labeled as "A" in the Fig. 17(iii). Via contour and also the physical structure of the vortex, we can say that at "A", the reduction of vortex strength has been achieved where the structured vortex which appeared in base case, has been physically change in hole cases.

For Fig. 17(iv), as the interaction between vortex continues, the strong vortex concentration which appear at base case are gradually disappeared in hole case (at trailing edge surface). Significant comparison has been observed at the surface area, where the hole has been added. Even in the base case, there is relatively low strength of the vortex at suction side and when a series of micro-hole has been added to this area, the vortex seems to be well distributed along the spanwise of the blade. As the result, this has reduced the vortex strength in the wake, make the vortex separated from initial vortex. Further downstream, the same effect as previous figure become more significant. Strong contour vortex which has been appeared in the base case, has been suppressed in the hole case. We can see there is no concentrated and "structured" vortex appeared at downstream of the hole case. Beside, a delayed in downstream vortex formation has been achieved.

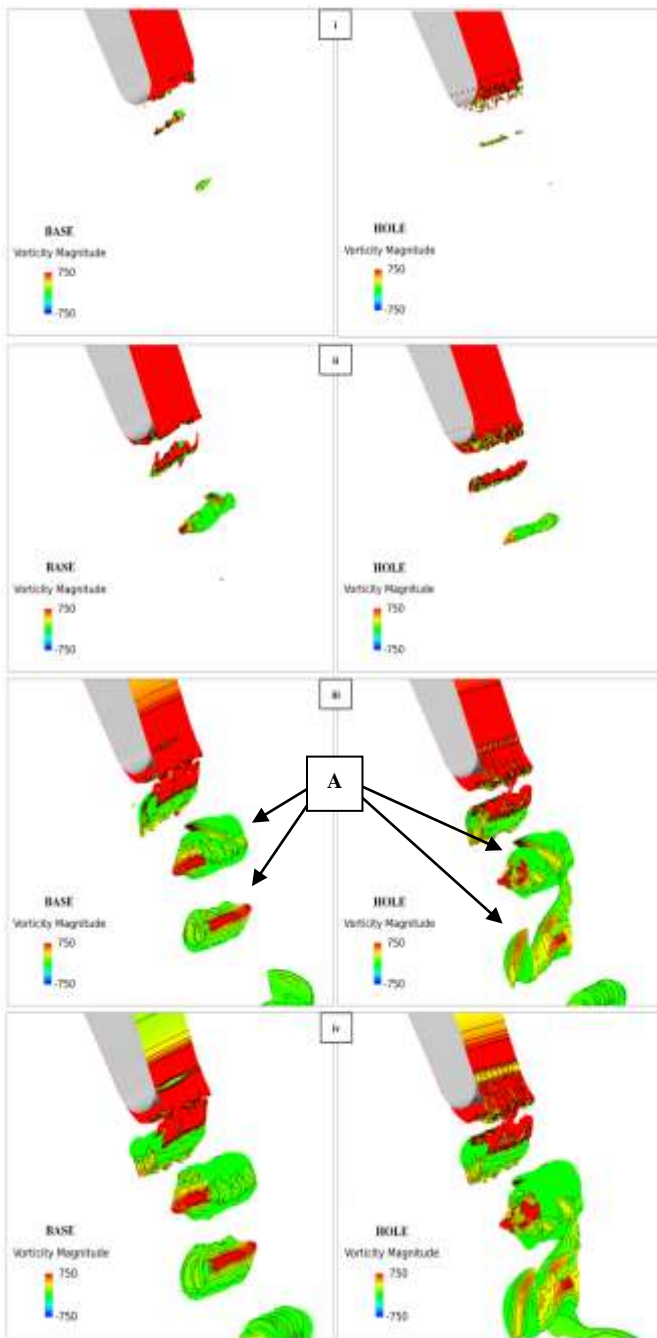


Figure 17. Iso-surface instantaneous vorticity magnitude for base and hole case. Hole case condition ($D_h = 0.094D$, $S/D = \pm 0.62$)

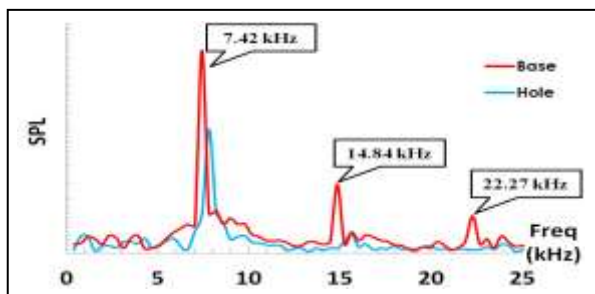


Figure 18. Frequency comparison between base and hole case. Hole case condition ($D_h = 0.094D$, $S/D = \pm 0.62$)

Fig. 18 shows the comparison of frequency between hole and base. Obviously, we can see the frequency has reduced dramatically (for hole case), especially for 2nd and 3rd peak. In a nutshell, added a series of micro-hole reduced the vortex formation at trailing edge surface initially, lead to reduce the strength of the vortex at the blade wake. Further downstream, it also observed that delayed in vortex formation.

iv. Conclusion

The application of a series of micro-hole on a turbine blade was numerically investigated. The turbulence model selection was a vital step in order to obtain an accurate result, where finally *SA-DDES* turbulence model has been chosen in this calculation. First, the effect of the hole size has been investigated. The larger hole diameter of $0.094D$ is the best among three other diameters. $D_h = 0.094D$ has reduced the wake loss at maximum of 10%, increase the trailing edge pressure distribution of 14% and gives a reduction in wake velocity profile thickness at maximum of 24% as compared with the base (no hole) case. Also, a series of micro-hole suppresses the vortex and reduces the pressure drop in the wake at lower distances of x/D .

Then, the effect of the location at fixed diameter hole of $0.094D$ has been studied. The best location is obtained at $S/D = \pm 0.62$, where the maximum reduction of average wake loss approximately 2.6% has been achieved, compared with the base case. The location of the hole also plays an important role, at the upstream location ($S/D = \pm 0.73$) has weakly affected the pressure distribution and wake loss, which the result is almost similar to the base case. In contrast, at the downstream location ($S/D = \pm 0.58$), the wake loss has been reduced 2.4%, as compared with the base case, which almost similar with the result at $S/D = \pm 0.62$. So we can conclude that, placing a series of micro holes at downstream of $S/D = \pm 0.62$ is effective for vortex suppression.

Upon this research scope, a micro-hole series of $D_h = 0.094D$ at $S/D = \pm 0.62$ has shown the best result among others, where the flow field also shows the suppression of vortex at downstream of the blade wake.

Acknowledgment

We are grateful for the Ministry of Higher Education (MOHE) and University of Technology MARA (UiTM) scholarship to Author 1.

References

- [1] James, P. L., 1990, Flow Separation Prevention on a Turbine Blade in Cascade at Low Reynolds Number, PhD Dissertation, Air Force Institute of Technology, AFIT/DS/ENY/99-01.
- [2] Shaker, S.F., Abdullah, M.Z., Mujeebu, M.A., Ahmad, K.A. and Abdullah, M.K., 2012, "Study On The Effect of Number Of Film Cooling Rows on The Thermal Performance of Gas Turbine Blade", Journal of Thermal Science and Technology, Vol.32, pp.88-98.
- [3] Zhang, X.F. and Hodson, H., 2010, "Effect of Reynolds Number and Freestream Turbulence Intensity on the Unsteady Boundary Layer Development on an Ultra-High-Lift Low Pressure Turbine Airfoil", ASME Journal of Turbomachinery, Vol.132, pp.1001-1010.

- [4] Denton, J.D., 1993, "Loss Mechanisms in Turbomachines", ASME Journal of Turbomachinery, Vol. 115, pp. 621-656.
- [5] Giovanni, N., 2011, Suppression of vortex shedding from a truncated trailing edge by plasma actuation, TUDelft, MSc Thesis, pp.5-23.
- [6] Bernardini, C., Carnevale, M., Manna, M., Martelli, F., Simoni, D., and Zunino, P., 2012, "Turbine Blade Boundary Layer Separation Suppression via Synthetic Jet: An Experimental and Numerical Study", Journal of Thermal Science, Vol. 21, No. 5, pp.404-412.
- [7] Zhou, C., Hudson, H. and Christop, H., 2014, "The Effects of Trailing edge thickness on the losses of Ultrahigh lift Low Pressure Turbine Blade", ASME Journal of Turbomachinery Vol.136, pp.1-12.
- [8] Dwayne, A.B., Steven, L.C., and David, R.D., 2005, "Vortex Shedding from a Hydrofoil at High Reynold Number", Journal of Fluid Mechanics, Vol. 531, pp.293-324.
- [9] Bearman, P.W., 1965, "Investigation of the flow behind a two-dimensional model with a blunt trailing edge and fitted with splitter plates", Journal of Fluid Mechanics. Vol. 21, Part 2, pp.241-255.
- [10] Yangwei, L., Jinjing, S. and Lipeng, S., 2014, "Corner Separation Control by Boundary Layer Suction Applied to a Highly Loaded Axial Compressor Cascade", MDPI Journal Energies, Vol.119, pp.786-793.
- [11] Kurmanov, B., Namba, M., and Podvidz, G., 2003, "Turbulent Flow Computation in Film-Cooling Turbine Cascade", Proceedings of the International Gas Turbine Congress 2003 Tokyo, pp.1-8.
- [12] El-Gendi, Mohammed, K.I., Mori, K., and Nakamura, Y., 2010, "Novel Flow Control Method of Vortex Shedding for a Turbine Blade", Transaction Japan Society of Aeronautic Space Science, Vol. 53, pp.122-129.
- [13] Sieverding, C.H., Ottolia, D., Bagner, C., Comodoro, A., Brouckaert, J.F., and Desse, J., 2004, "Unsteady Turbine Blade Wake Characteristics", ASME Journal of Turbomachinery, Vol.126, pp.551-559.
- [14] Sieverding, C.H., Richard, H. and Desse, J., 2003, "Turbine Blade Trailing Edge Flow Characteristics at High Subsonic Outlet Mach Number", ASME Journal of Turbomachinery, Vol.125, pp.298-309.
- [15] Blazek, J., 2001. Computational Fluid Dynamics; Principles and Applications, Elsevier, pp.267-293.
- [16] Clark, J.P., and Grover, E.A., (2007). "Assessing Convergence in Predictions of Periodic-Unsteady Flow Fields", ASME Journal of Turbomachinery, Vol. 129, pp.740-749.
- [17] Azebedo, M.A., Cavadas, A.S., Coelho, P.M., Proenca, M.F. and Pinho, F.T., 2012, "Control of vortex shedding behind a circular cylinder at moderate Reynolds number", Proceedings of Conferência Nacional em Mecânica dos Fluidos, Termodinâmica e Energia, pp.1-9
- [18] Cerri, G., Giovannelli, A., Battisti L., and Fedrizzi, R., "Advances in effusive cooling techniques of gas turbine", Journal of Applied Thermal Engineering, Elsevier, Vol. 27, pp.692-698.
- [19] Lipowsky, H., Kovalcheck, S., and Zweifach, B.W., (1978), "The distribution of blood rheological parameters in the microvasculature of cat mesentery", Circulation Res, Issue 43, pp.738-749.
- [20] Skalak, R., 1990, Capillary Flow: Past, Present and Future, Biorheology, No.27, pp.277-293.
- [21] Loudon, C., and McCulloh, K., 1999, "Application of the Hagen-Poiseuille Equation to Fluid Feeding Through Short Tubes", Entomological Society of America, Vol. 92, No. 1, pp.153-158.
- [22] Spalart, P.R., and Allmaras, S.R., 1992, "A One-Equation Turbulence Model for Aerodynamics Flows", 30th Aerospace Sciences Meeting & Exhibition, January 1992, pp.1-22
- [23] Deck, S., Duveau, P., D'Espiney, P., and Guillen, P., 2002, "Development and application of Spalart-Allmaras One Equation Turbulence Model to Three Dimensional Supersonic Complex Configuration", Elsevier Aerospace Science and Technology, No. 6, pp.171-183.
- [24] Spalart, P.R., Jou,W.-H., Strelets, M., and Allmaras, S.R., 1997, "Comments on the feasibility of LES for wings, and on a hybrid RANS/LES approach", Advances in DNS/LES, pp.137-147
- [25] Spalart, P.R., Deck, S., Shur, M.L., Squires, K.D., Strelets, M.K. and Travin, A., 2006, "A New Version of Detach-Eddy Simulation, Resistant to ambiguous Grid Densities", Theoretical Computational Fluid Dynamics, Vol.20, pp.181-195.
- [26] Chai, X., and Manesh, K., 2010, "Dynamic k-Equation Model for Large Eddy Simulation of Compressible Flow", AIAA 2010-5026, pp.1-13.
- [27] Deardorff, J.W., 1970, "A Numerical Study of Three-Dimensional Turbulent Channel Flow at Large Reynolds Number", Journal of Fluid Mechanics, Vol. 41, Part 2, pp.453-480
- [28] Potsdam, M., and Pullian, T., 2008, "Turbulence modeling treatment for rotorcraft wakes". In AHS Specialist's Conference on Aeromechanics, Jan. 23-25.
- [29] M.El-Ghondour, Shatat, M.M.E., and Nakamura, Y., 2012, "On the physics of Vortex Formation at the Tip of a Turbine Blade", ASME Turbo Expo 2012: Turbine Technical Conference and Exposition, June 11-15.
- [30] Magagnato, F., and Gabi, M., 2008, "Prediction of Transitional Flow of Turbine Blades with DDES and LES", Proceedings of 8th World Congress on Computational Mechanics, July 2008.
- [31] Friedrichs, S., Hodson, H.P., and Dawes, W.N., 1999, "The Design of an Improved Endwall Film-Cooling Configuration", ASME Journal of Turbomachinery, Vol.121, pp.772-780.
- [32] Shan, J.W., and Dimotakis, P.E., 1968, "The Turbulent Mixing in Transverse Jets", Proceedings of the 3rd Australasian Conference on Hydraulics and Fluid Mechanics, pp.159-163.
- [33] Saha, A.K. and Shrivastava, A., 2015, "Suppression of Vortex Shedding around a Square Cylinder using Blowing", Sadhana Springer, Vol.40, pp. 769-785.
- [34] Mulleners, K., Gilge, P. and Hohenstein, S., 2014, "Impact of surface roughness on the Turbulent Wake Flow of a Turbine Blade", Journal of Aerodynamics, pp.1-9.
- [35] Effendy, M., Yao, Y., and Yao, J., 2003, "Comparison Study of Turbine Blade with Trailing-Edge Cutback coolant Ejection Designs", Proceeding of 51st AIAA Aerospace Science Meeting including the New Horizons Forum and Aerospace Exposition, pp. 1-12.
- [36] Collie, J.C., Moses, H.L., Schetz, J.A. and Geogory B.A., 1993, "Recent Advances in Simulating Unsteady Flow Phenomena Brought About by Passage of Shock Waves in a Linear Turbine Cascade", ASME Journal of Turbomachinery, Vol. 115, pp.687-698.
- [37] Lutum, E. and Johnson, B.V., 1999, "Influence of the Hole-to-Diameter ratio on Film Cooling with cylindrical hole", ASME Journal of Turbomachinery, Vol.121, pp.209-216.
- [38] Bunker, R.S., 2005, "A Review of Shaped Hole Turbine Film-Cooling Technology", ASME Journal of Heat Transfer, Vol. 127, pp.441-453.

About Author (s):



Mohd Hafiz Mohd Noh received his Bachelor degree in Mechanical Engineering from University of Technology Tun Hussien Onn Malaysia (UTHM) 2005 and Master Degree in Master of Science (Aerospace Propulsion) from Cranfield University, UK. At present, he is pursuing his PhD at Fluid Dynamics Lab, Department of Aerospace Engineering, Nagoya University Japan. His research interest is in CFD, Turbomachinery and Heat Transfer.



Koichi Mori received his Master Degree from University of Tokyo, Japan and PhD from University of Tokyo, Japan. He is a member of Japan Society of Aeronautics and Astronautics Japan and Japanese Applied Physics Society. At present, he is working as Associate Professor at Fluid Dynamics Lab, Department of Aerospace Engineering, Nagoya University Japan. His research interest is in Fluid Dynamics, Advanced Space Propulsion and Laser Technology.